Testing beam-induced quench levels of LHC superconducting magnets

B. Auchmann, T. Baer, M. Bednarek, G. Bellodi, C. Bracco, R. Bruce, F. Cerutti, V. Chetvertkova, B. Dehning, P. P. Granieri, W. Hofle, E. B. Holzer, A. Lechner, E. Nebot Del Busto, A. Priebe, S. Redaelli, B. Salvachua, M. Sapinski, R. Schmidt, N. Shetty, E. Skordis, M. Solfaroli, J. Steckert, D. Valuch, A. Verweij, J. Wenninger, D. Wollmann, and M. Zerlauth

CERN, 1211 Geneva 23, Switzerland

(Received 19 February 2015; published 25 June 2015)

In the years 2009–2013 the Large Hadron Collider (LHC) has been operated with the top beam energies of 3.5 and 4 TeV per proton (from 2012) instead of the nominal 7 TeV. The currents in the superconducting magnets were reduced accordingly. To date only seventeen beam-induced quenches have occurred; eight of them during specially designed quench tests, the others during injection. There has not been a single beam-induced quench during normal collider operation with stored beam. The conditions, however, are expected to become much more challenging after the long LHC shutdown. The magnets will be operating at near nominal currents, and in the presence of high energy and high intensity beams with a stored energy of up to 362 MJ per beam. In this paper we summarize our efforts to understand the quench levels of LHC superconducting magnets. We describe beam-loss events and dedicated experiments with beam, as well as the simulation methods used to reproduce the observable signals. The simulated energy deposition in the coils is compared to the quench levels predicted by electrothermal models, thus allowing one to validate and improve the models which are used to set beam-dump thresholds on beam-loss monitors for run 2.

DOI: 10.1103/PhysRevSTAB.18.061002 PACS numbers: 29.27.Eg, 41.85.Lc

I. INTRODUCTION

During the LHC run 1 (2009–2013) a total of 17 beam-induced quenches were observed. Most quenches occurred during dedicated experiments (quench tests) or at beam setup time. The operational quenches took place exclusively during the injection process [1]. The low number of beam-induced quenches in comparison to other superconducting accelerators (HERA [2], Tevatron [3], and RHIC [4]) is explained by a better orbit stability, efficient beam-tail cleaning, sophisticated interlocks, and the low magnet currents of about half the design value. In 2015, after the long shutdown 1 (LS1), the LHC will be running at nominal energy and more frequent beam-induced quenches are expected. Therefore a good understanding of quench levels for various beam-loss scenarios is important, where a beam-loss scenario is determined by the affected magnet, its working point, the loss duration, and the geometrical loss pattern.

The quench level is defined as the minimum local energy or power deposition that, for a given beam-loss scenario, will result in a transition from superconducting to normal-conducting state. Electrothermal models are used to estimate the quench level. Most calculations for the LHC have been based on the phenomenological model in [5]. Direct validation by measurement, however, is difficult as spot heaters on the coil invariably alter the cooling of the strands. In 1977 at FNAL a magnet was installed in a beam line for test purposes. The energy deposition was measured *a priori* by means of a calorimeter representing the coil [6]. Here, we attempt to reproduce the actual beam-loss event by means of simulation, validate the numerical model with observable monitoring signals, and take from the model the corresponding energy or power deposition in the coils [7]. The 17 beam-induced quenches in the LHC can serve to estimate quench levels in the quenching magnets. Adjacent magnets that did not quench, as well as beam-loss events that did not result in quenches at all, can serve to estimate lower bounds on quench levels. From all events, in this paper we study those that represent a relevant beam-loss scenario, that result in an energy or power deposition in the coils sufficiently close to the assumed quench level, and that produce enough quality data for the validation of numerical models. The findings are compared to electrothermal estimates of quench levels for the respective beam-loss scenario.

In this paper we present the current status of our efforts in understanding quench levels using the example of six events, five of which were dedicated quench tests at the end of the LHC Run 1, covering a variety of beam-loss scenarios. In each case we describe the beam-loss event, explain the particle-tracking (where applicable) and the particle-shower simulations and their validation with event

data, and study the consistency of electrothermal quench-level estimates with the obtained information. In Sec. II we introduce terminology as well as a classification of beam-loss scenarios according to loss duration. Section III describes the numerical analysis procedures used throughout the paper. The quench-test results are analyzed in Secs. IV for short-duration losses, V for intermediate-duration losses, and VI for steady-state losses. Section VII summarizes the findings.

II. QUENCH LEVELS

The quench level is a measure of the maximum amount of energy or, in the steady-state case, power that can be deposited locally in a superconducting magnet without provoking the transition to a normal-conducting state. The quench level is a function of the local magnetic field, the operating temperature, the cooling conditions, the geometrical loss pattern, and the time distribution of the beam losses. There are three main regimes, distinguished by the duration t of the beam losses.

A. Short-duration ($t < 50\ \mu$s)

The local quench level is determined predominantly by the volumetric heat capacity of a dry cable, with little effect of cooling to liquid helium. The quench level in this regime is quantified by the minimum quench energy density (MQED) and measured in $\mathrm{mJ/cm^3}$. In the short-duration regime, the maximum value of energy deposition across the cable cross section is relevant. This typically coincides with the location of the lowest margin to quench in the cable. The collimation quench test and the injection-study event, described in Secs. IV A and IV B, respectively, probe quench levels at the submicrosecond scale at different magnet working points.

B. Intermediate duration ($50\ \mu\mathrm{s} \lesssim t \lesssim 5$ s)

The liquid helium in the cable interstices and, to a lesser extent, around the insulated conductor plays a crucial role; see Fig. 1 and Sec. III. This is due to the efficient heat transfer to and the large heat capacity of liquid helium.

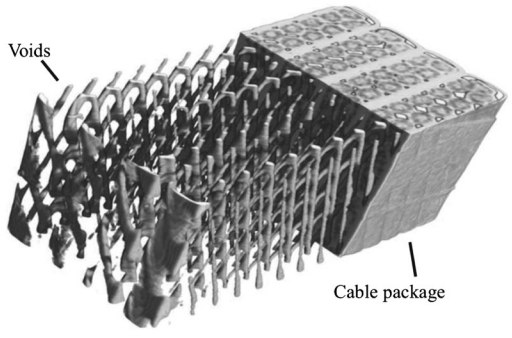

FIG. 1. 3D image from neutron tomography of cable interstices in a stack of Rutherford-type cable [8].

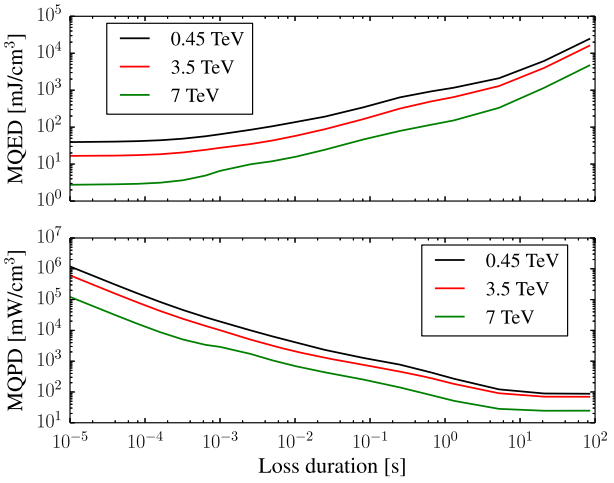

FIG. 2. MQED (up) and MQPD (down) as a function of beam-loss duration for heat pulses of constant power. The quench levels are computed with QP3 [9] on the horizontal plane of a main-dipole magnet, for the geometrical loss pattern of [10], with magnet currents corresponding to injection beam energy (450 GeV), 3.5 TeV, and 7 TeV.

In the intermediate-duration regime, the quench level is expressed by the above-mentioned MQED. It depends on the actual distribution of energy deposition across the cable. The wire-scanner quench test in Sec. V A and the orbit-bump quench test in Sec. V B investigate this regime.

C. Steady state ($t > 5$ s)

The heat is constantly removed with a rate that is mainly determined by the heat transfer to the helium bath through the cable insulation. The quench level, in this case, is expressed as a minimum quench power density (MQPD) and measured in $\mathrm{mW/cm^3}$. MQPD is given as an average density across the cable cross section. The collimation quench test in Sec. VI A and the orbit-bump quench tests in Secs. VI B and VI C cover the steady-state regime. To illustrate the dependence of the MQED and MQPD on the loss duration, Fig. 2 shows simulation results of the QP3 code [9] for a main dipole magnet on the horizontal plane, and for the geometrical loss distribution described in [10]. It can be seen that in the short-duration regime, MQED is constant and MQPD is linear with loss duration, whereas in the steady-state regime MQPD is constant and MQED is linear. This graph was used to define the time ranges for this paper.

III. METHODOLOGY

Despite the different causes of beam losses in the studied quench tests and operational events, the analysis procedures are similar in all cases. The measurement data is provided mainly by the beam-loss monitors (BLM), the quench protection system (QPS), the beam position monitors (BPM), and the fast beam-current transformer

(FBCT). The numerical analysis proceeds along the following steps.

1. The geometric loss pattern on a suitable interface is calculated with MAD-X [11] or SIXTRACK [12]. SIXTRACK, in addition to magnetic tracking, includes also a Monte Carlo of the proton-matter interaction in the collimators, which allows multiturn tracking including outscattering. The interface between tracking and particle-shower simulations may be the beam-screen surface, or a transverse plane, e.g., the frontal plane of a collimator. On the interface, the position and momentum distribution of the particles serves as an input for particle-shower simulations, which may continue the tracking to the point where the particles hit dense matter. Particle tracking with MAD-X or SIXTRACK may cover the moment of maximum losses, a steady-state regime, or all the beam manipulations leading up to the beam loss.

2. Particle-shower simulations with FLUKA [13,14] or GEANT4 [15] are used to estimate the energy deposition in the BLMs' active volume and inside the superconducting coil. Longitudinally, the simulation may cover a single magnet or a whole section of the accelerator. Radially the simulated geometry extends to the tunnel walls. Particle-shower simulations provide distributions of deposited energy per impacting proton. The normalization of the simulation results is done by means of the total loss in beam intensity as measured by the FBCTs. The energy deposition in the BLMs is compared to the measured signal. Good agreement gives confidence in the simulated energy deposition in the coils. A full account of the methodology and related uncertainties of particle-shower simulations related to LHC beam operation is given in [16].

3. An electrothermal simulation with QP3, THEA [17], or ZERODEE [18] yields quench level estimates in the most critical position of the coil. QP3 and THEA are one-dimensional codes, taking the distribution of losses along a strand into account, whereas the averaging assumptions of ZERODEE make it suited for strand-wise computations in the short-duration regime, and cable computations in the steady-state regimes only. Both, QP3 and THEA, provide different options to take the cooling to helium inside the cable into account. For the same assumptions, they yield identical results. Electrothermal estimates presented in this paper are based on the heat-transfer models documented in [19]. For the intermediate and steady-state regimes, the BLM signal provides the time profile of the heat pulse in the coils. The time profile is curtailed at the moment a resistive voltage is visible in the QPS data. The radial loss profile across the cable from FLUKA, the temporal profile of losses from the BLM signals, and the magnetic field distribution across the cable from ROXIE [20] at the given magnet current are taken into account. Note that only relative, not absolute values of BLM signals and FLUKA simulations are used as input to the electrothermal model. The influence of the radial distribution from FLUKA on the electrothermal quench-level estimate is significant only in the intermediate-duration regime, where it may change the computed MQED by several ten percent.

4. If no quench occurred in the simulated event, particle-shower simulations provide a lower bound for the quench level. If a quench occurred, the energy deposition based on the total number of protons lost in the event provides an upper bound. For intermediate-duration and steady-state losses, the determination of the moment of quench during the beam loss period allows one to determine the number of protons lost at the moment of quench, and, thus, to deduce a direct estimate of the quench level. Consistency between particle-shower simulations and quench-level estimates increases the confidence in the electrothermal model as well as in the overall understanding of the event.

5. The electrothermal model can be used to extrapolate the quench level estimate to similar events at different magnet currents.

Figure 3 illustrates the analysis process. Both the numerical simulations and the experimental data are affected by errors. We mention the most important ones.

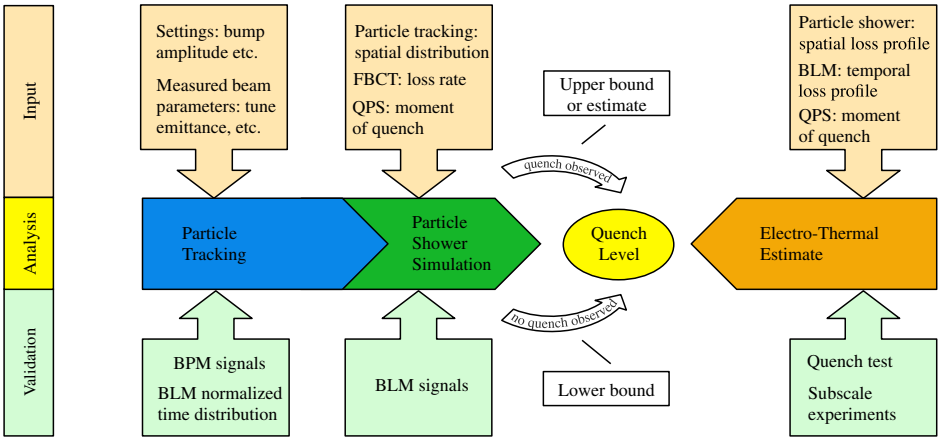

FIG. 3. Overview of the analysis methodology for quench tests.

Electrothermal models are affected by three major uncertainties: (1) In the intermediate-duration regime, the model features multiple mechanisms of heat transfer between the strands and the helium filling the voids in the Rutherford cable (Kapitza cooling, convection cooling, nucleate and film boiling, etc.). Models and parameters vary widely in literature. For this paper we use two distinct models described in [21] (Sec. 2.2) and [22], respectively. The differences in the results are presented as an uncertainty range in this paper. (2) Mostly affecting the intermediate-duration regime is the amount of helium in the interstrand voids of the Rutherford cable, as well as the area of contact between strands and helium. Tomographic imaging was used in [23] (p. 59 and following) and the results were in agreement with previous measurements in [24]. In [22], the more pragmatic assumption is made that half of the geometric void area is filled with helium (the other half being filled with the Kapton insulation), and that 50% of the strand diameters are in contact with helium. (3) Experimental work on the heat extraction through the cable insulation in the steady-state regime has been carried out at CERN [25–27]. The experimental data used in the QP3 and THEA codes is described in [26]. More experimental work is under way to confirm and extend this data set, in particular with regard to the efficiency of the intralayer spacers in the LHC main magnets [28].

Particle-shower simulations rely on an approximation of the equipment and tunnel geometries, as well as material distributions therein. Simulations that require a model of an extended section of the accelerator cannot be modeled with the same level of detail as those that require only one or two magnets. The geometry of coil ends is not accurately modeled in FLUKA, so that energy depositions in the magnet ends are not evaluated with the same accuracy as those in the magnet straight sections. Cases that result in a pronounced peak in energy deposition may suffer from the averaging over evaluation cells that are usually 10 cm long. Statistical errors are typically negligible. GEANT4 simulations of several of the quench tests are discussed in [29]; to make their models more generic, the authors assumed a constant impact angle of particles on the beam screen. Here we present work with FLUKA in which each model attempts to represent the actual events and tests as accurately as possible. More detailed information is found in [16].

Particle-tracking uncertainties arise from an idealized description of the machine and imperfect knowledge of initial conditions. Geometric parameters such as tolerances on the beam-screen geometry, surface roughness, and misalignment affect the results. Additional uncertainties in the case of SIXTRACK come from the simulation of particle-matter interactions in collimator jaws.

QPS data is provided for system monitoring at 5 ms intervals. For losses in the intermediate-duration regime this sampling rate makes a precise determination of the moment of quench difficult; see point III above. The synchronization of BLM data and QPS data is affected by a similar uncertainty of 5–10 ms.

BLMs that are exposed to large energy deposition draw high currents from their power distribution line. In rare cases this may affect the reading on other BLMs on the same power-distribution line.

IV. SHORT-DURATION LOSSES

The most likely loss scenario in this regime is an injection failure or an asynchronous beam dump. The quenches induced by fast beam losses at injection are described in [10,30]. While an injection failure will quench magnets, the collimation system and the QPS protect the magnets from damage; the BLM system is used for *a posteriori* diagnostics. As for asynchronous beam dumps, the most affected magnets are the quadrupoles close to the dump kickers called Q4 and Q5 (wide-aperture quadrupoles), operating at 4.5 K. A study of quench levels for the short-duration regime is used to set trigger levels for abort-gap cleaning [31]. In the following, two beam-induced quenches are investigated: first, an actual event from the first commissioning with beam, and then a dedicated quench test to probe quench levels in the short-duration regime.

A. Strong-kick quench event

1. Experimental setup

Out of several beam-induced quenches which took place at injection [1], an event of 9th September 2008 is presented here. In this event, a main dipole (MB.B10R2 operating at 1.9 K) in the dispersion suppressor region, equipped with several BLMs, was quenched in an attempt to reproduce an accidental quench that occurred a few weeks earlier during an aperture scan in the arc downstream of interaction region 2 (IR2). The earlier quench concerned a different magnet. The measurement consisted of injecting a pilot bunch (few 10^9 protons), inducing trajectory oscillations with various amplitudes by means of a vertical corrector (MCBCV.9R2), and monitoring the downstream losses. The beam was then stopped at a collimator in the momentum cleaning insertion (IR3). A large vertical kick of nominally 750 μrad was applied at the corrector and 2×10^9 protons hit directly the MB.B10R2 aperture, inducing a quench.

2. Particle tracking

The reconstruction of the trajectory of the kicked beam was done with MAD-X by matching the calculated trajectory with the actual BPM measurements. The strengths of the correctors, which were employed to correct the trajectory to the reference one, were used as matching variables (the range is $\pm 20\%$ of the applied strength). The initial beam coordinates (x_0, x_0', y_0 and y_0') were used to

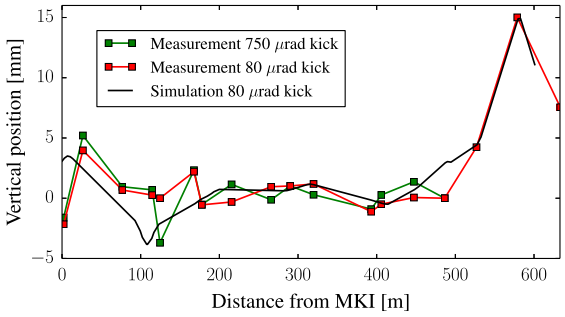

FIG. 4. Vertical trajectory of the injected beam. Black line: MAD-X simulation of injection with 80 μrad kick by MCBCV.9R2 vertical orbit corrector. Red line: BPM readings for of 80 μrad kick. Green line: BPM readings for 750 μrad kick.

better fit the BPM signals, thus, accounting for possible injection errors [32].

For the shot which caused the quench, no BPM data was available downstream of the MCBCV.9R2 orbit corrector (green line in Fig. 4, the corrector is located at 494 m from the injection kickers MKI) since the beam was lost due to the large kick. Data from a previous injection, with an applied kick of 80 μrad, was used as reference for the matching and a reasonable agreement with measurements was found as shown in Fig. 4. These calculations allowed one to define the position of the beam (± 1 mm accuracy) at the vertical corrector and the real strength of the kick (714 μrad $\pm$ 10%) given to the beam when the quench occurred.

3. Particle-shower simulation

A transverse plane at the beginning of the MCBCV.9R2 orbit corrector acted as the interface between MAD-X and FLUKA simulations. The coordinates and momenta at the interface were used as starting values in the FLUKA energy deposition studies in the dipole located 24 m downstream. Figure 5 (up) shows the measured maximum BLM signals compared to the simulated maximum BLM signals during the event. The agreement observed for all the downstream BLMs is within 20%. In this particular event, BLM signals are very sensitive to uncertainties in the vertical coordinates at the interface between particle-tracking and particle-shower simulations. Figure 5 (down) shows the maximum deposited energy density along the coil. The energy deposition in the coil is very sensitive to the horizontal angle at the interface.

The resulting energy density map is shown in Fig. 6. The maximum energy density in the coil is about 36 mJ/cm^3, which occurs very close to the vertical plane. For the beam emittance a conservative estimate of 1 μm rad was used. If the emittance were smaller, the maximum energy density in the coil could have been higher. For a vertical kick of a beam on the design trajectory, the maximum of the deposited energy density would have been found

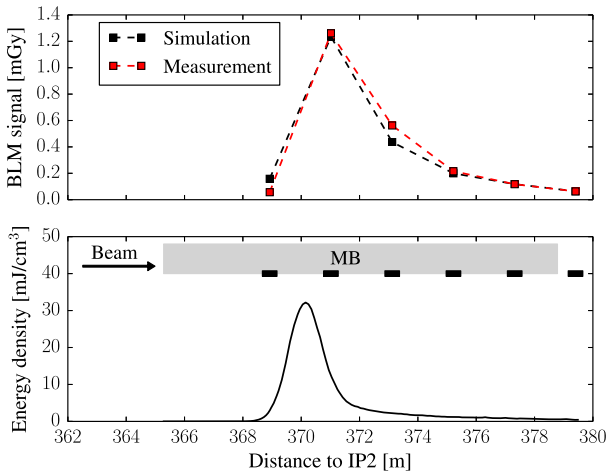

FIG. 5. Up: Comparison of BLM signals measured during the strong-kick event and simulated with FLUKA. Beam direction is from the left to the right. Down: FLUKA simulated peak energy deposition in the coils, integrated over the event. The gray box indicates magnet cold mass, black boxes indicate the location of BLMs.

in the magnet collar; due to oscillations of the beam after injection, the maximum energy density is moved into the magnet coil. This effect accounts for a large part of the discrepancy with analysis results presented in [10] (p. 37).

4. Electrothermal simulation

Results of FLUKA and of electrothermal analyses are shown in Table I. The losses being instantaneous, helium cooling does not play a role in the electrothermal model. The MQED can be calculated directly from the effective

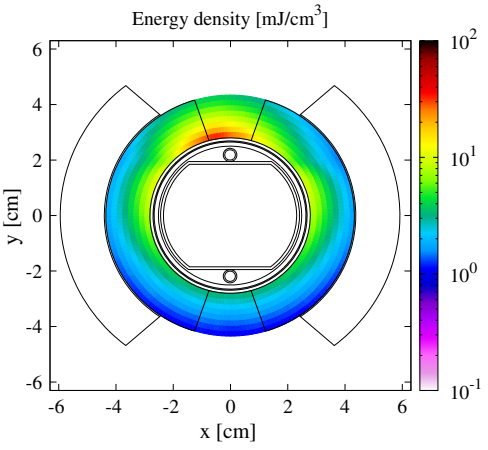

FIG. 6. Simulated transverse energy density distribution from FLUKA for the strong-kick event in MB.B10R2 coils at the position where the maximum energy deposition occurs. Results correspond to 2×10^9 protons impacting on the magnet beam screen. Spatial coordinates are with respect to the center of the vacuum chamber.

TABLE I. Quench-level comparison; FLUKA upper bound and the electrothermal MQED estimate for the strong-kick event.

Particle shower calculation mJ/cm^3	Electrothermal estimate $[mJ/cm^3]$
≤ 36	38

heat capacity of the strand according to NIST material data [33,34]. The electrothermal simulation codes agree with the value thus obtained. The uncertainty in the particle tracking induces an uncertainty in the FLUKA simulations, which may well account for the small discrepancy between the upper bound obtained from FLUKA and the calculated MQED.

5. Discussion

The simulation of beam losses due to a kick or an orbit-bump requires an accurate model of the beam dynamics leading up to the loss. We will encounter this effect in later sections. In the present case, not enough information is available to reduce the uncertainty on the FLUKA upper bound value. It should be noted that we cannot generally expect an accuracy at the 10% level. We trust the electrothermal MQED estimate, which depends only on the strand enthalpy and the critical temperature; see "short-duration" in Sec. II.

B. Dump on injection absorber

1. Experimental setup

In order to further study fast-loss events, a quench test was devised that caused an injected bunch at 450 GeV to be dumped directly on an injection-protection collimator (TCLIB). At the same time, the individually powered matching-quadrupole magnet (MQM at 4.5 K) Q6.L8 in the shadow of the collimator was powered at varying current levels. The TCLIB jaws were closed to a gap between the jaws of ~1 mm, corresponding to the anti-collision limit which prevents the jaws from touching, and an offset was applied with respect to the beam center to intercept the full injected beam. An oscilloscope was installed on the MQM magnet for enhanced diagnostics to record voltages across the magnet with higher time resolution than the QPS system could.

A first test of this kind was performed in July 2011 [35] using a maximum bunch intensity of 3×10^{10} protons and a magnet current of up to 2200 A. The oscilloscope registered a voltage spike at each injection. An offline analysis showed that the spike amplitude varied linearly with bunch intensity. No correlation was found with the magnet current. A normal transition with subsequent fast recovery could, thus, be excluded. The test was repeated in February 2013. The bunch intensity was 6.5×10^{10} protons and the current was increased in steps of 500 A until a quench occurred at 2500 A, which corresponds to operation at 6 TeV. The 2011 observations on voltage spikes were confirmed. The mechanism causing the spikes is not fully understood at this point.

2. Particle-shower simulation

The energy deposited in the coils was estimated by means of FLUKA simulations, reproducing the actual impact conditions on the collimator. The simulations included an accurate representation of TCLIB, Q6, TCLIM (a mask upstream of Q6), and corresponding aperture transitions. The strength of the quadrupole field was adjusted according to the magnet current applied in the test. Owing to the jaw length of 1 m and the active absorber material that is graphite, approximately 90% of the impacting protons experienced an inelastic nuclear interaction inside the jaws, while only 10% of the incident proton energy were absorbed in the TCLIB.

Comparison of FLUKA results with BLM data proved impracticable. BLMs in the vicinity of TCLIB and MQM saturated. Further downstream, the agreement was not good; the measured BLM signal was 20 times lower than the simulated one. As mentioned above, data from BLMs on a common power distribution line may be unreliable if a large number of BLMs reach saturation.

For the quench event at 2500 A the FLUKA model predicted a maximum energy density of 31 mJ/cm^3 on the magnet coils. A similar peak energy density of 29 mJ/cm^3 was deposited at the lower current of 2000 A, when no quench was observed; see Table II. Statistical errors are less than 2%. Figure 7 shows that the simulated losses were distributed over the length of the magnet, with a maximum in the straight part of the magnet. Owing to the larger horizontal elongation of the beam, the maximum energy density was registered in the horizontal plane on the inner coil diameter. This is illustrated in Fig. 8, showing the transverse energy density distribution in the inner and outer layers of the MQM coils.

3. Electrothermal simulation

The results of FLUKA and of electrothermal analyses are shown in Table II. The losses being instantaneous, helium cooling does not play a role in the electrothermal model. As above, the MQED is calculated directly from the effective heat capacity of the strand. Comparison between the lower

TABLE II. Quench-level comparison; FLUKA bounds and the electrothermal MQED estimate for the short-duration collimation quench test.

Current [A]	Particle shower calculation $[mJ/cm^3]$	Electrothermal estimate $[mJ/cm^3]$
2000	>29	20
2500	≤ 31	16

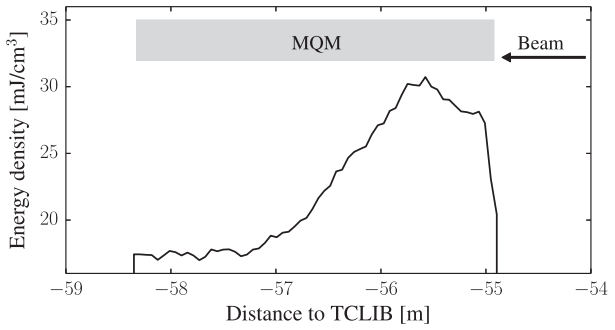

FIG. 7. FLUKA simulated peak energy density deposited in the coil during the short-duration collimation quench test. The gray box indicates the magnet.

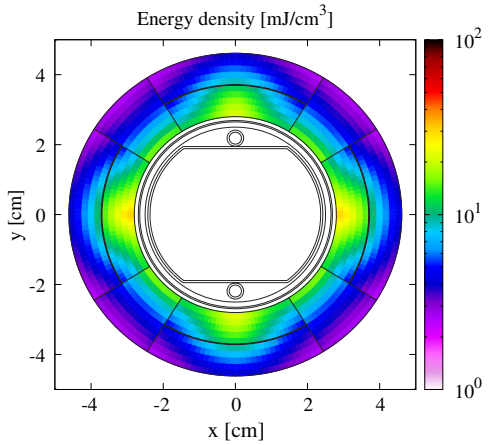

FIG. 8. Simulated transverse energy density distribution for the short-duration collimation quench test in the Q6.L8 coils (2500 A) at the position where the maximum energy deposition occurs.

bound for MQED given by FLUKA simulations at 2000 A, and the corresponding electrothermal MQED estimates shows a mismatch by a factor of roughly 1.5.

4. Discussion

The quench test was to serve as a benchmark for the FLUKA model and the electrothermal model. It is unfortunate that the BLM data was saturated. In a future experiment, BLM types with higher dynamic range should be used. Nonetheless, from the result we can learn about the necessary safety factors that may need to be applied in the calculation of fast-loss BLM thresholds which are based on similar FLUKA models based on loss scenarios for which BLM data does not yet exist for validation.

V. INTERMEDIATE-DURATION LOSSES

LHC operation in the years 2010–2013 was affected by a phenomenon of millisecond-duration beam losses. The time structure of the losses, as observed by the BLM system, was approximately Gaussian. These losses are suspected to be provoked by dust particles getting in the way of the beams [36–39]. Dust particles can be encountered anywhere around the ring. Statistically, the most frequent single location is at the injection kickers, affecting mainly the wide-aperture quadrupole (MQY at 4.5 K) Q5. Falling dust particles somewhere in the arcs' main bending (MB) and main quadrupole (MQ) magnets, covering tens of kilometers of the LHC, are expected to be the most critical type of beam losses. During LS1, one out of three BLMs on the short straight sections in the arc has been relocated to improve the detection of losses related to dust particles in the arcs. No quench was provoked during run 1 and no correlation has been found between beam energy and the occurrence of dust particles. However, the MQED after LS1 is estimated to be 2–4 times smaller, while the energy deposition due to beam interaction with dust particles is expected to be 2–3 times higher [40]. This makes dust particles a prime candidate for beam-induced quenches after LS1. New BLM thresholds have to be determined for the new BLM locations based on the numerical models and test results presented in this section.

Other beam-loss scenarios of intermediate duration include sudden current variations in magnet circuits, or losses on collimators at certain stages of beam operation (end of ramp, squeeze). Fast changes in magnet currents, in particular on certain warm magnet circuits [41], are intercepted by a system of fast magnet-current monitors. The BLM system can intervene as a second line of protection, dumping the beam after the machine-protection system's design response time of 270 μs or three turns.

Two experiments were designed to investigate the quench level for intermediate-duration losses: the wire-scanner quench test [42] and the orbit-bump quench test.

A. Wire-scanner quench test

1. Experimental setup

One way to generate millisecond losses of roughly Gaussian shape in a controlled way is to use the wire scanner as a source of beam loss. Such an experiment was performed in November 2010 using the wire scanner installed on beam 2. This beam was chosen because the collimation region downstream of the wire scanner prevents potential propagation of the losses around the ring.

The beam intensity was $N_p = 1.53 \times 10^{13}$ protons contained in 144 bunches at a beam energy of 3.5 TeV. The wires in the scanners are made of carbon fiber with a diameter of $d_w = 30$ μm. They perform a linear movement with a nominal speed of 1 m/s. During the experiment the speed of the wire v_w was gradually decreased with each scan with the sequence: 1, 0.75, 0.5, 0.37, 0.3, 0.25, 0.2, 0.15, and 0.05 m/s, when finally a quench occurred.

The magnet which quenched was a separation dipole D4.L4 (MBRB type at 4.5 K and 3070 A) placed about 33 m downstream of the wire scanner. In the same cryostat,

there is a quadrupole magnet Q5.L4B2 (MQY type at 4.5 K and 1094 A), which had also been a potential candidate for quenching. Eight BLMs were installed on these magnets.

The quench of the D4 triggered an acquisition of signal buffers, which are presented in Fig. 9. The non-Gaussian shape of the loss registered by the BLMs suggests that the wire movement was not linear and that vibrations occurred together with wire sublimation. Similar behavior of the wires in extremely intense beams was observed before [43]. Indeed the investigation of the wire after the experiment revealed sublimation of 50% of wire diameter in the location of the beam impact. The slow rise of the QPS signal is indicative of a quench due to an energy deposition close to the quench level in the magnet ends in the low-field region of the coil.

A precise determination of the moment of quench is difficult due to the long sampling intervals of the QPS data and the uncertainty in the synchronization of individual signals. These uncertainties affect the particle-shower simulation of the energy deposited in the coil at the moment of quench, as well as the electrothermal MQED estimate.

2. Particle-shower simulation

For a normal scan of a Gaussian beam the amount of protons passing through the wire N_w can be expressed by [16]

$$N_w = N_p \cdot f_{LHC} \cdot d_w / v_w, \quad (1)$$

where $f_{LHC} = 11$ kHz is the revolution frequency of protons in the LHC, v_w the wire velocity, d_w the wire diameter, and N_p the number of protons in the beam. In order to estimate the actual number of protons interacting with the wire in the last, irregular scan, we use an unexpected increase of the integrated BLM signal. For all preceding scans we had found that the product of wire speed and BLM signal S_{BLM} was constant, $S_{BLM} \cdot v_w =$ const. Moreover, with N_w from Eq. (1), we had found that N_w was proportional to the BLM signal, $N_w \propto S_{BLM}$. For the last scan, $S_{BLM} \cdot v_w$ was 30% higher than expected. This finding translates to an estimated N_w of 1.3×10^{14} protons.

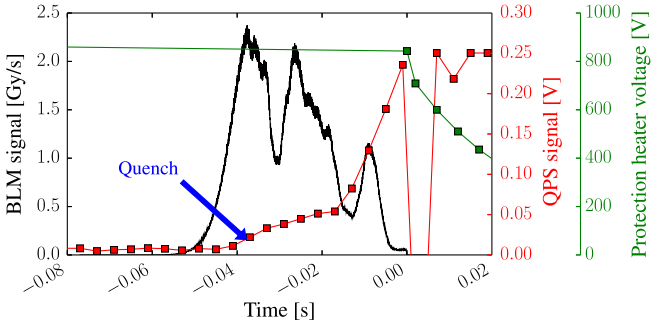

FIG. 9. BLM (black) and QPS (red) signals registered during the orbit-bump quench test with intermediate loss duration. A drop in QPS heater-voltage indicates heater firing (green), which was synchronized with the moment of beam dump. The QPS signal measures resistive voltage in a magnet. The 0.1-V intercept of the QPS signal was timed to precede the heater firing by 10 ms, i.e., the QPS evaluation time.

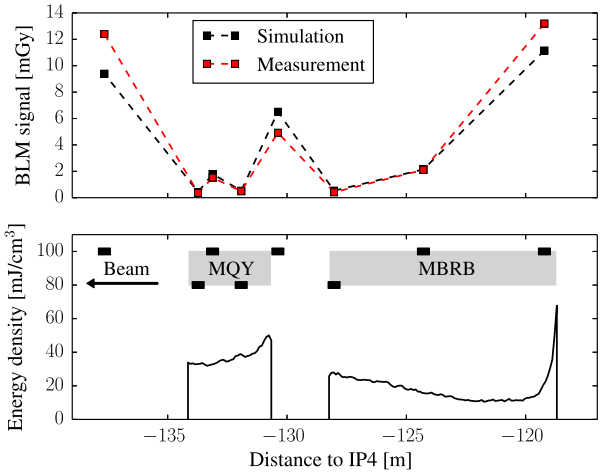

FIG. 10. Up: Comparison of integrated BLM signal accumulated during the wire-scanner quench test and simulated with FLUKA. Down: FLUKA simulated peak energy density deposited in the coils over the entire event. Gray boxes indicate magnet cold masses, black boxes indicate the locations of BLMs.

The agreement in shape and amplitude of FLUKA simulations with BLM data [see Fig. 10 (up)] was very good, thus, vindicating the above considerations. The uncertainties affect the calculation of the energy deposited in the coil at the moment of quench. In the MBRB, the peak energy deposition occurred in the coil end; see Fig. 10 (down). This makes a precise determination of the locally deposited energy in the magnet coil difficult. FLUKA results are shown in Tables III and IV. The corresponding transverse energy-deposition in the MBRB coils is shown in Fig. 11.

3. Electrothermal simulation

MQED estimates for the beam-loss scenario presented by the wire-scanner quench test are affected by the uncertainty on the moment of quench in the same way

TABLE III. Quench-level comparison; FLUKA estimate and electrothermal MQED estimate in the MBRB coil for the wire-scanner quench test. Lower values in electrothermal estimates correspond to a reduced cooling model; upper values correspond to the standard cooling model.

v_w [m/s]	N_q/N_w [%]	Particle shower [mJ/cm^3]	Electrothermal [mJ/cm^3]
0.15	...	>18	26–37
0.05	30	20	25–35
0.05	45	30	26–42

TABLE IV. Quench-level comparison; FLUKA bound and the electrothermal MQED estimate in the MQY coil for the wire-scanner quench test.

v_w [m/s]	Particle shower calculation [mJ/cm^3]	Electrothermal estimate [mJ/cm^3]
0.05	>50	52

as FLUKA simulations, thus, adding an uncertainty to N_q, the number of protons lost until the MBRB magnet quenched for $v_w = 0.05$ m/s. A synchronization of signals as shown in Fig. 9 means that $N_q/N_w = 30\%$; if the quench occurred 5 ms later (recall that 5 ms is the QPS sampling rate) we find $N_q/N_w = 45\%$. For the quench test with $v_w = 0.15$ m/s no quench occurred. The BLM signals are not available, so we assume a horizontal beam distribution with $\sigma_h = 300$ μm and, consequently, a Gaussian time distribution with $\sigma_t = \sigma_h/v_w = 2$ ms. Since the FLUKA model of the MBRB does not feature an accurate geometrical model of the coil ends, the location of quench and, hence, the magnetic field in the location of quench are not well known. Moreover, due to the filling of gaps in the magnet ends with putty, the cooling conditions in the ends are little known. Tables III and IV show the simulation results. The lower MQED estimate corresponds to a situation with no helium cooling and higher local magnetic field, whereas the higher MQED value considers the standard model as it would be applied in the straight section of the magnet. The maximum in the loss distribution inside the MQY coils is 10 cm inside the magnet coil. We therefore assume standard cooling and field conditions in the MQY. The fact that the magnets are operated at 4.5 K means that the helium inside the cable plays a lesser role than, for instance, in the orbit-bump quench test in Sec. V B.

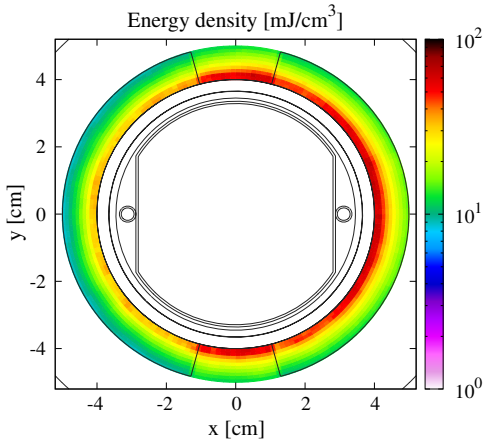

FIG. 11. Simulated transverse energy density distribution from FLUKA, integrated over the event, in D4.L4 coils at the location where the maximum energy deposition occurs during the intermediate-duration orbit-bump quench test.

4. Discussion

The wire scanner is an ideal device to generate millisecond-duration losses with a Gaussian loss profile. Its position in the ring allows one to create losses in the D4 magnet that are sufficiently intense to make the magnet quench. Unfortunately, the relative position of wire scanner and D4 is such that the peak losses occur in the magnet ends, making an accurate simulation rather difficult. The test is not likely to be repeated due to the limited supply of spare magnets for the D4. A similar experiment on a magnet cooled to 1.9 K would be desirable. The losses, in that case, would have to be considerably higher (see the following section), and the wire scanner would have to be fitted for the purpose. In any case, any experiment in the intermediate-duration regime should record BLM and QPS signals with an oscilloscope to avoid timing issues in the analysis.

B. Orbit-bump quench test

1. Experimental setup

The LHC transverse damper (ADT) [44] can be used not only to damp beam oscillations but also to excite the beam by so-called operation in sign-flip mode, which gives kicks to selected bunches. The preparation of the beam excitation procedure for the orbit-bump quench test is described in [45]. First, a three-corrector orbit bump was applied in the horizontal plane around the main quadrupole MQ.12L6 (at 1.9 K). Second, the tune kicker (MKQ) kicked the bunch horizontally. Third, with a delay time of 1 ms or 11 turns, the horizontal ADT started the excitation of a single bunch in sign-flip mode. Two attempts were made. Both times the entire bunch containing $N_p = 4 \times 10^8$ protons in the first try and $N_p = 8.2 \times 10^8$ in the second try was lost into the magnet. The second attempt resulted in a quench in the magnet. A particular challenge lay in the measurement of the beam intensity and the emittance of bunches with several 10^8 protons per bunch, which is more than 10 times below the design sensitivity of the LHC beam instrumentation.

In Fig. 12 the recorded BLM and QPS signals of the second attempt are presented. The total duration of losses was about 10 ms, with loss spikes roughly every four revolutions of the excited bunch. The determination of the precise moment of quench suffers from the low sampling rate (5 ms) of QPS data and the imperfect synchronization of BLM, heater, and QPS signals. For this purpose, an oscilloscope was installed, which, however, stopped operating during the first attempt, possibly due to radiation issues. For MQED estimates, we assume that the quench occurred after about 5 ms when about $N_q = 5.3 \times 10^8$ protons were lost; see the caption of Fig. 12.

The particular shape of the QPS signal allows for two different interpretations. The QPS signal is the difference between two voltages, each measured across two poles of

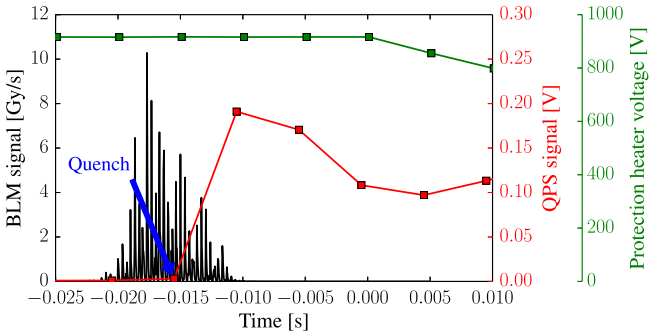

FIG. 12. BLM (black) and QPS (red) signals registered during the orbit-bump quench test with intermediate loss duration. A drop in QPS heater-voltage indicates heater firing (green), which was synchronized with the moment of beam dump. The QPS signal measures resistive voltage in a magnet. The 0.1-V intercept of the QPS signal was timed to precede the heater firing by 10 ms, i.e., the QPS evaluation time.

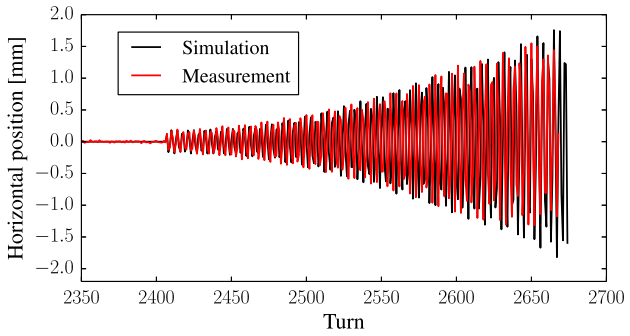

FIG. 13. Comparison of MAD-X simulation and data collected by a beam-position monitor during the intermediate-duration orbit-bump quench test.

the affected quadrupole. Since the QPS signal has a local minimum at $\sim +5$ ms (see Fig. 12), the magnet may be recovering to a superconducting state before the protection heaters become effective. Quench recovery in an MQ at 4 TeV and the corresponding magnet current is, however, very unlikely. Alternatively, the second voltage signal may be "catching up" to the first signal, due to an almost symmetric quench development across the two pairs of voltage taps. For such cases, an additional layer of protection is provided by the symmetric quench protection system that compares voltages across apertures of adjacent magnets.

2. Particle tracking

This quench test required a much more detailed particle-tracking study than the single-turn and fixed-target losses described so far. Extensive tracking studies with MAD-X [11] have been performed to model the spatial as well as the time distribution of losses on the beam screen from the excited bunch [46]. In order to fully describe the experimental conditions, the simulations strictly followed the chronology of the experiment: the orbit bump was followed by an MKQ kick, and the ADT excitation. The BPM data in the position of the ADT was used for tuning the strengths and directions of the MKQ and ADT kicks in the MAD-X model. In the simulation, the ADT kick is treated as a sine function with growing amplitude for the first 100 turns, and constant amplitude thereafter, corresponding to a saturation of the ADT kick strength. In Fig. 13 the simulated beam position at the BPM is compared to the experimental data. The time, position, impact angle, and energy of every particle touching the aperture is stored. The results of the tracking simulations are used as input for FLUKA particle shower simulations; see Fig. 14 (down).

Parametric studies revealed that the largest uncertainties in the particle-tracking results are due to the imperfect knowledge of tune and beam profile, moments before the beam losses occurred. The maximum in the spatial loss distribution may be 20% lower if the tune after establishment of the three-corrector bump was 64.268 rather than the nominal 64.274 or, alternatively, if the beam was twice as wide. The amplitude of the orbit bump, when increased, shortens the overall longitudinal loss distribution; however, since the maximum of the loss distribution remains unchanged, this variation leaves BLM signals and the peak energy distribution in the coils unchanged.

Particle-tracking results for orbit-bump scenarios were systematically checked for their sensitivity to tiny discontinuities in the beam-screen surface, e.g., a region of elevated surface roughness. This type of imperfection was modeled as a 20-cm-long aperture restriction of 30 μm height. The effect of the restriction depends largely on how fast the

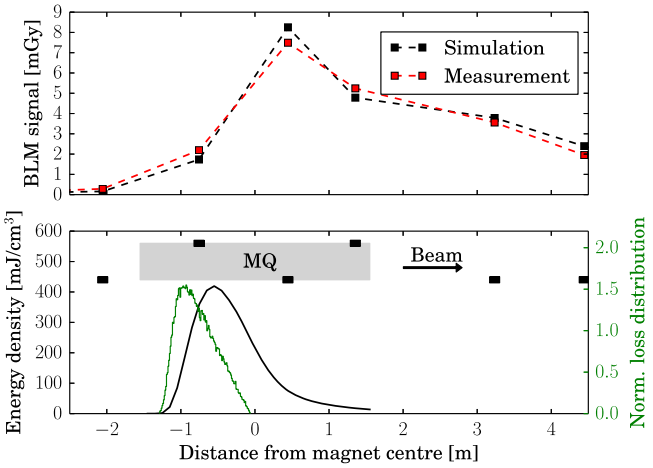

FIG. 14. Up: Detail of the comparison between the BLM signal, accumulated during the intermediate-duration orbit bump quench test, and the simulated signal from FLUKA. Down: FLUKA simulated peak energy density deposited in the coils (black) and MAD-X histogram of protons lost on the beam-screen (green), normalized to the total number of simulated lost particles. The gray box indicates the magnet, black boxes indicate the locations of BLMs.

beam is driven towards the aperture. To generate losses in the millisecond time range, the combined MKQ and ADT kicks cause a relatively wide loss distribution, with a maximum towards the beginning of the magnet; compare Fig. 14 with Fig. 22, where the latter shows a similar event but with slow beam blowup over 20 s. The impact angle varies linearly along the length of the quadrupole [46] (Fig. 1). As a consequence, an aperture restriction at the beginning of the magnet shields a short downstream section from impacting protons, whereas a restriction towards the magnet center can effectively curtail a loss distribution. From this reasoning, and the loss distribution shown in Fig. 14, it follows that orbit-bump tests with strong kicks are not highly sensitive to small aperture restrictions. Moving the restriction along the magnet causes either a shorting at the end, or a prolongation at the beginning of the distribution; however the change in overall results (including the subsequent particle-shower simulation) does not exceed 10% for the assumed roughness height of 30 μm.

While the spatial loss distribution showed low sensitivity to parameter changes, the time structure of losses varied more strongly. Since the beam was excited for a short time only, its blowup could be neglected, besides excitation happened too fast in order to allow for cutting the phase-space ellipse along its perimeter. Therefore the envelope of the loss peaks had a Gaussian-like shape, reflecting the shape of the beam profile. The frequency of the loss peaks strongly correlates with the tune. The duration of the loss depends on the beam size and on the orbit bump amplitude. An accurate reproduction of the time structure observed in the BLM signals could not be achieved. The likely reasons are the above-mentioned uncertainties in the tune and the beam profile measurements, as well as higher-order effects.

3. Particle-shower simulation

The MAD-X simulations predict a spatial loss distribution which is restricted to a 1.2-m-long area upstream of the longitudinal magnet center. The impact angles of protons on the magnet beam screen gradually decrease from the beginning towards the center of the magnet, owing to the focusing quadrupole field. The MAD-X loss distribution was integrated over time, and used as an input for FLUKA shower calculations [47]. Figure 14 (up) compares simulated and measured signals for a string of BLMs positioned along the cryostat of the impacted quadrupole magnet. For BLMs located downstream of the assumed loss location, the agreement between simulation and measurement is found to be better than 30%.

Parametric studies involving both, FLUKA and MAD-X, have been carried out. The peak energy deposition in the coil was shown to correlate with the peak in the geometrical distribution of lost particles on the beam screen. The energy deposition in the location of the BLMs was considerably less sensitive. Sharp peaks and more drawn-out distributions on the beam screen produce in the BLMs nearly identical signatures, owing to the very forward direction of the particle shower.

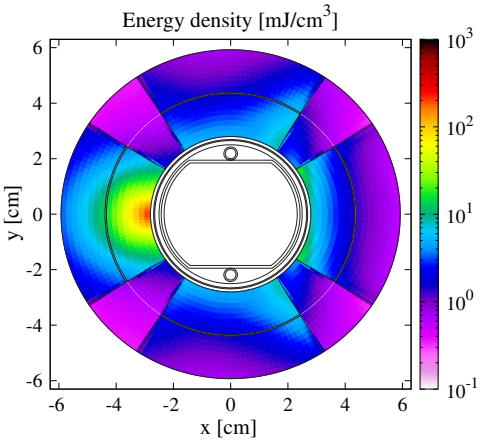

FIG. 15. Simulated transverse energy density distribution from FLUKA in MQ.12L6 coils at the location where the maximum energy deposition occurs during the intermediate-duration orbit-bump quench test. Results correspond to 4×10^8 protons impacting on the magnet beam screen.

Figure 15 illustrates the transverse energy density profile at the position of the maximum energy deposition. The displayed distribution corresponds to a cumulative loss of $N_p = 4 \times 10^8$ protons. Lower bounds are imposed by the intensity of bunches used in tests without quench, $N_p = 4 \times 10^8$. For a bunch intensity of $N_p = 8.2 \times 10^8$ protons, the experiment resulted in a quench. Owing to the limited time resolution of the QPS signals, the number N_q of protons impacting on the beam screen up to the moment of quench cannot be determined conclusively. For $N_q = 5.3 \times 10^8$ protons lost, corresponding to the assumption that the magnet quenched after 5 ms of losses (see Fig. 12), the estimated maximum energy density is about 265 mJ/cm^3; see also Table V. An upper bound to the quench level is given by $N_q = N_p$, which results in an MQED of 405 mJ/cm^3.

TABLE V. Quench-level comparison; FLUKA calculations and electrothermal estimates of the MQED in the MQ coil for the intermediate-duration orbit-bump quench test. Lower values in the electrothermal estimate correspond to a more pessimistic cooling model; both cooling models neglect a potential increase of cooling power by an enhanced nucleate-boiling regime.

N_p	N_q	Particle shower [mJ/cm^3]	Electrothermal [mJ/cm^3]
4×10^8	n/a	>198	61–71
8.2×10^8	5.3×10^8	265	50–58
8.2×10^8	8.2×10^8	≤405	70–80

4. Electrothermal simulation

The radial distribution of losses determined by FLUKA is normalized to the maximum value and used for the loss profile in the electrothermal simulation. For the time distribution, the BLM signals were normalized to their maximum value and truncated at the presumed moment of quench. Simulation results are shown in Table V. We find that the electrothermal model appears to underestimate the quench level in this regime substantially. Several effects have been discussed in this context: A thin helium film all around the affected strand could increase the cooling capability in the first instances of losses considerably; current redistribution could delay the measurable resistive signal, even though the longitudinal peak is relatively broad for this effect to play a decisive role (see Fig. 14); nucleate boiling has been shown, albeit in a semi-infinite bath, to be highly effective on very short time ranges [48]. Numerical studies show that if we allow the cooling model to fall back to the nucleate-boiling regime after each short loss peak, the observed values could be roughly reproduced. In the absence of a comprehensive fluid-dynamic model, however, this observation is merely the ground for speculations. This enhanced nucleate-boiling regime was not used for the values presented in Table V. We need more experimental and theoretical work to arrive at a predictive model of helium cooling with superfluid helium in Rutherford-type cable in the intermediate-duration loss regime. Note that the wire-scanner quench test, which was carried out on a magnet operated at 4.5 K, did not show this kind of underestimation.

5. Discussion

The experiment succeeded in generating losses over several milliseconds that resulted in a magnet quench. The quench occurred in the straight section of the magnet, thus avoiding a problem observed in the wire-scanner quench test. The particular time structure of losses, with peaks roughly every 300 μs, represents an important deviation from the Gaussian-shape losses due to dust particles. The experiments may, therefore, not be all-together suitable to draw conclusions on limitations due to falling dust particles for LHC operation. As in the case of the wire-scanner quench test, we note that oscilloscope recordings of BLM and QPS signals are mandatory for any future test.

VI. STEADY-STATE LOSS QUENCH TESTS

Steady-state losses are generated by luminosity debris hitting magnets close to the experiments, and by collimators in the cleaning insertions. These losses cannot be avoided therefore they set limits to the machine performance. Residual particle showers from the collimation system constitute a well-defined scenario, directly amenable to experimental testing. The 2011 and 2013 collimation quench tests were performed with protons and ions [49,50] without quenching, thus, providing a lower bound on the quench level, i.e., on MQPD. Five tests using the orbit-bump technique with protons resulted in quenches. Here we present the 2013 collimation quench test with protons in Sec. VI A, and orbit-bump quench tests in Secs. VI B and VI C, which test the quench level in main quadrupoles for increasing and near-constant power deposition, respectively.

A. Collimation quench tests

1. Experimental setup

During regular LHC operation, the dispersion suppressor magnets (DS) in IR7 are the superconducting elements that are most exposed to beam losses leaking out of the betatron collimation system [51–54]. These losses, together with the beam lifetime, limit the maximum beam intensity that can be injected. Dedicated collimation quench tests were devised to explore this limit in the DS regions.

In 2011, two tests were performed, with protons and ions, respectively, at 3.5Z TeV [50,55]. The main goal was to achieve a loss rate of 500 kW which is the maximum loss rate the collimation system was designed to intercept [51]. Beam losses on the collimators were triggered for beam 2 over 1 s by crossing the third-order resonance to blow up the beam. The fraction of particles leaking from the collimators into the DS region, as well as their impact distribution, stayed the same as in standard operation, while the number of lost particles increased significantly. The method allowed one to investigate performance limitations due to the DS magnets' quench level. The leakage, however, was not high enough to provoke a quench.

In this paper, we describe the more recent experiment performed in 2013 with protons at 4 TeV; see also [56]. In order to increase the losses in the DS of IR7 with respect to the 2011 tests, the collimator settings were changed. We adopted the relaxed collimator settings used during the 2011 run, and opened further the secondary collimators in IR7. The global effect of these changes was to increase the number of impacts in the DS of IR7 for the same beam loss. The optimization of the settings was the result of the combination of tracking studies with SixTrack [12,57–59], and a detailed validation during a low-intensity fill before the quench test.

Beam losses on the primary collimator (TCP in IR7) were generated by blowing up the beam with white noise from the ADT [44]. This mechanism allowed to generate beam losses that increased continuously over 10 s. Figure 16 shows the peak power loss during the 2011 and the 2013 tests. Beam losses of up to 1050 kW were generated in the last ramp with up to 5.8 MJ impacting on the primary collimator over a few seconds. During that period the BLM signals were monitored. As in 2011, no magnet quench occurred. The maximum BLM signals in the cold sector were measured at the position of the main quadrupole MQ.8L7.

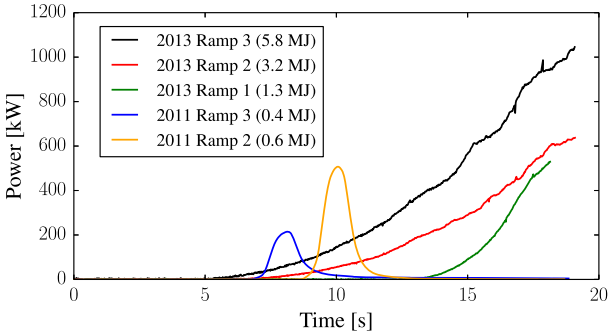

FIG. 16. Measured peak power losses by the beam in the collimation system versus time during the collimation quench tests in 2011 and 2013. In 2013 tests, beams were dumped after achieving the targeted loss rate.

2. Particle tracking and shower simulation

Dedicated simulations with SixTrack and FLUKA were performed after the test. The distribution of proton losses (i.e., inelastic events) over the IR7 collimators computed by SixTrack, using COLLTRACK/K2 [57,58] routines, was used as a source term for FLUKA calculations; see [59]. The latter ones incorporated a very detailed 700 m long geometry model and allowed to evaluate the deposited energy density in the DS magnet coils as well as the BLM signals. Results were normalized to the achieved loss rate, as measured by the FBCT.

In Fig. 17 (down), the peak power density in the inner superconducting coils is plotted along the length of the most impacted magnets. The maximum is on the front face of the first dipole in cell 9. Figure 17 shows the corresponding power density map on the magnet transverse section. The horizontal plane is mainly affected, due to the particle shower originated from protons experiencing a limited energy loss and angular kick (typically a diffractive event) in the primary collimator, leaking through the collimation system down to the DS, where they are overbent by the magnetic field towards the internal boundary of the physical aperture.

Figure 17 (up) presents the comparison between measured and predicted BLM signals in the region considered here. Values are normalized to the signal of the BLM at the skew primary collimator, since measurements refer to an integration time over which the loss rate was not constant. The shortest integration time of 40 μs could instead be used for the much higher experimental signals in the collimator region, allowing there an absolute comparison confirming the full consistency of the normalization factors adopted here [16]. A more exhaustive presentation of the FLUKA model and the comparison to measurements is found in [60]. Despite a remarkable agreement globally achieved over the whole IR7 insertion, calculations feature a localized underestimation of a factor of a few from the end of the long straight section up to cell 9 (as in Fig. 17). Such an underestimation may reasonably imply that the power density in the magnet coils was actually higher than in Figs. 17 and 18.

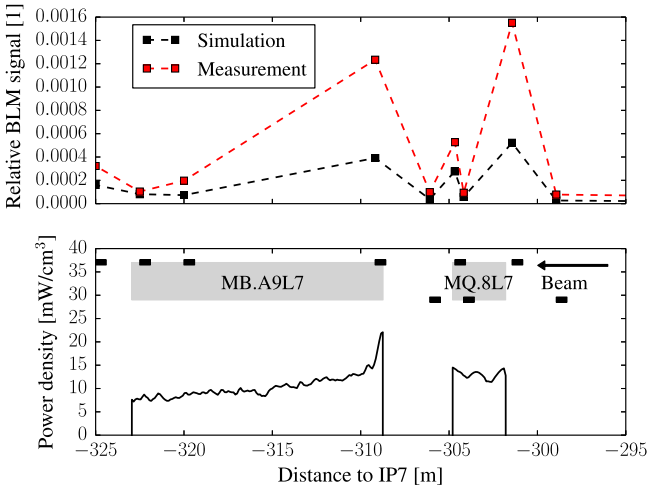

FIG. 17. Up: Local excerpt of the comparison of BLM signals and FLUKA simulation results for ramp 3 of the 2013 collimation quench test, both respectively normalized to the BLM of the skew primary collimator (TCP.B6R7) located at +200 m [16,60]. Down: Longitudinal pattern of the power density (averaged over the inner coil radial thickness) at the transition between cells 8 and 9.

3. Electrothermal simulation

In the steady-state regime, the quench level depends on the effectiveness of the cooling to the helium bath, which was tested in dedicated experiments [26]. The experiments determine the temperature rise in a stack of ten cables under continuous heating. The stack is submerged in superfluid helium at 1.9 K and exposed to pressures of up to 100 MPa. In most magnets, the cables that are exposed to beam losses

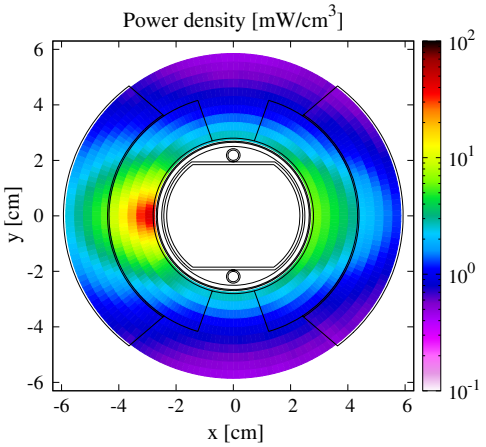

FIG. 18. Simulated transverse power density distribution from FLUKA during the steady-state collimation quench test at the MB.A9L7 maximum in Fig. 17 (down). The beam direction enters the figure. Recall from Sec. III that in FLUKA coils are extruded, not adequately representing the coil ends.

are cooled only on the inner diameter. LHC main dipole and quadrupole magnets, however, are equipped with an intralayer spacer that is slotted in order to provide channels for the superfluid helium. In [27], the slots in the intralayer spacer are assumed to be ideally effective until the strands reach the lambda temperature, i.e., the temperature when the helium in the cooling channels in the Kapton insulation stops to be superfluid. Moreover, an average pressure of 50 MPa was assumed. A more conservative model neglects the cooling to the interlayer helium and assumes 100 MPa on the inner diameter of the heated cable. The results from both assumptions are shown in Table VI. Both models are consistent with the lower bound obtained from the collimation quench test. According to the FLUKA model, the peak of the losses was deposited in the ends of the MB magnet. As a consequence, the exact magnetic field and the cooling conditions in the position of peak losses are not accurately known; compare with a similar discussion in Sec. V A.

4. Discussion

The collimation quench test closely reproduces an operational scenario. The relevant relationship between losses on the collimator and maximum power deposition in the magnet coils is difficult to simulate. The large-scale FLUKA model shows overall remarkable performance [60]. In the high-loss region in the cold section of the model, however, the agreement is not satisfactory. Moreover, as the peak losses occur in the magnet ends, there are additional uncertainties due to simplifications in the geometrical model in FLUKA and the limited knowledge of cooling conditions and local magnetic field in the electrothermal model. Only an actual quench can give more certainty in this beam-loss scenario. Nonetheless, the large-scale particle-shower model is a major step forward in our capabilities to analyze distributed events. As for the electrothermal model, no additional insights could be gained on the efficiency of the cooling slots in the intralayer spacers of MB and MQ magnets.

B. Dynamic orbit-bump quench test

1. Experimental setup

The experiment was done at 3.5 TeV beam energy. A vertical three-corrector orbit bump was formed around the main (horizontally defocusing) quadrupole (MQ.14R2 at 1.9 K) and slowly increased for ∼10 s, until ∼60% of the initial 2.54×10^9 protons were lost and the magnet quenched [61,62]. The resulting BLM signal is shown in Fig. 19.

TABLE VI. Quench-level comparison of the FLUKA lower bound and the electrothermal MQPD estimate in the MB.A9L7 coil for the steady-state collimation quench test. The upper and lower values for the electrothermal estimate correspond to a cooling model with and without heat flow through the intralayer spacers, respectively.

Particle shower calculation [mW/cm^3]	Electrothermermal estimate [mW/cm^3]
>23	115–140

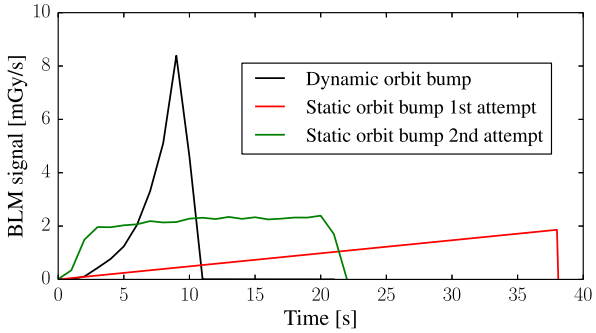

FIG. 19. Comparison of the highest BLM signal time profiles for the 2010 dynamic orbit-bump quench test and the 2013 static orbit-bump quench tests. Note that in 2013 static losses were only achieved in the second attempt.

2. Particle tracking

The spatial and time distributions of the lost particles were studied using MAD-X. A vertical orbit bump was applied around the quadrupole MQ.14R2. In the simulations the amplitude of the orbit bump was increased by 10 μm every 50 turns, reproducing the experimental conditions on a shorter time scale. Scaling the time axis of the normalized loss distribution to the actual loss duration provides a good qualitative fit to the normalized observed BLM signals.

3. Particle-shower simulation

The loss distribution obtained from the MAD-X simulation was used as a source term for the FLUKA simulation. The resulting particle shower was tracked and the energy density in the coils estimated. The number of protons lost in the last second before the dump, 2.54×10^9 protons/s, was used to scale FLUKA results. The resulting BLM signals and energy deposition are shown in Fig. 20. The agreement between simulation and measured BLM signals is excellent. Figure 21 shows the simulated transverse power density distribution in the coils. The maximum power density, averaged over the affected turn, is estimated to be 208 mW/cm^3.

4. Electrothermal simulation

The losses in the dynamic orbit-bump quench test were not actually steady state. In terms of peak power at the moment of quench, the acceleration of losses increased the quench level for this loss scenario. Two alternative models were used for steady-state cooling, differing in the assumption on the effectiveness of the interlayer cooling

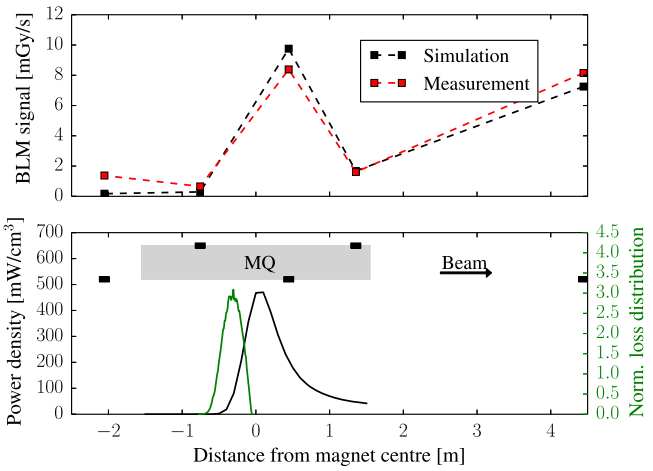

FIG. 20. Up: Detail of the comparison between the BLM signal and the simulated signal from FLUKA for the dynamic orbit-bump quench test. Down: FLUKA simulated peak energy density (black) deposited in the coils and MAD-X normalized distribution of protons lost on the beam screen (green). The gray box indicates the magnet, black boxes indicate the locations of BLMs.

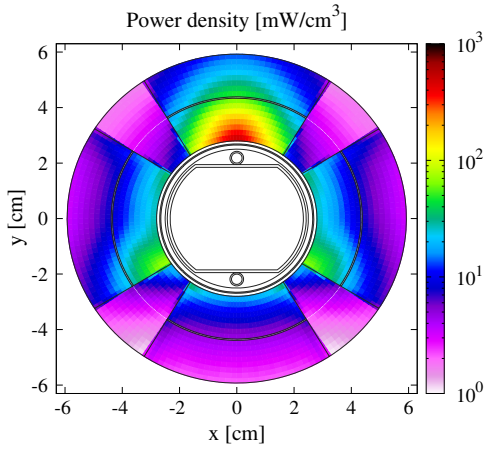

FIG. 21. Simulated transverse power density distribution from FLUKA during the dynamic orbit-bump quench test in MQ.14R2 coils at the position where the maximum energy deposition occurs. Results correspond to 2.54×10^9 protons impacting on the magnet beam screen. Spatial coordinates are with respect to the center of the vacuum chamber.

channels in the MQ. Results are displayed in Table VII. The agreement between FLUKA and electrothermal-model results is remarkably good. FLUKA values are within the range of known uncertainty of the electrothermal estimates.

5. Discussion

The dynamic orbit-bump quench test was the first of its kind, producing losses over several seconds before quenching the magnet. The good agreement between measured and simulated BLM data, as in the case of the intermediate-duration orbit-bump quench test, indicates a good grasp of the beam dynamics leading up to the quench, as well as the subsequent shower development. The good agreement with the electrothermal model, finally, makes this one of the best understood beam-induced quenches in the LHC.

TABLE VII. Quench-level comparison; FLUKA and the electrothermal MQPD estimate for the dynamic orbit-bump quench test. The integrated deposited energy is averaged across the cable cross-section. The upper and lower values for the electrothermal estimate correspond to a cooling model with and without heat-flow through the intralayer spacers, respectively.

Particle shower calculation mW/cm^3	Electrothermal estimate [mW/cm^3]
208	180–215

C. Static orbit-bump quench test

1. Experimental setup

A local orbit bump was established around a main quadrupole magnet (MQ12.L6 at 1.9 K), such that the beam almost touched the aperture. Eight low-intensity bunches of 1×10^{10} protons each were slowly blown up using white noise excitation in the ADT. The first attempt produced linearly rising losses over 38 s and no quench after 6.1×10^9 protons lost [29]. At the second attempt, after losing about 6.2×10^9 protons at a constant rate over 20 s, the magnet quenched. The corresponding BLM signals can be seen in Fig. 19. The linear rise during the first attempt is attributed, as in the dynamic-orbit-bump test, to the Gaussian beam profile. The losses are slow enough to cut off consecutive layers of the phase-space ellipse. The rising profile, therefore, corresponds to the tails of the distribution. The same bunches were used in the second attempt. In the absence of renewed beam-profile measurements, it is assumed that the remnants of the bunches diffused into a wider and more flat distribution in between the attempts, thus, explaining the flat loss profile over time observed in the second attempt.

2. Particle tracking

In order to reproduce the excitation of eight bunches in MAD-X, eight sets of simulations were performed, followed by a combined analysis. Each of the sets followed the same procedure: first, an equilibrium beam distribution with the experimentally measured sigma was created; second, the orbital bump was established around the focusing quadrupole MQ.12L6; and finally, the white-noise excitation with the ADT started. The sensitivity of the longitudinal distribution was tested with respect to the ADT kick strength and, as in the previous orbit-bump quench tests, to aperture restrictions. Additional studies have shown that increase of the kick strength leads to a decrease in the height of the distribution, a shortening of the loss

duration, and a longer longitudinal distribution. A weak value of ADT kick strength within the realistic parameter range produces the most realistic results. The impact angle depends only on the integral magnetic field of the quadrupole, seen by the particles.

In the subsequent particle-shower simulation moderate agreement of measured and simulated BLM signals was found; see Fig. 22. This came as a surprise, after the successful reproduction of BLM signals during the intermediate-duration orbit-bump quench test and the dynamic orbit-bump quench test. A study of the impact of small aperture restrictions was carried out to check whether a geometric effect of this kind could explain the discrepancy. A 20-cm-long and 30-μm-high step into the otherwise smooth aperture was found to have a strong influence on the overall loss distribution of particles. Since the impact angle of the particles is small, losses peak on the onset of the restriction, leaving the surface behind it in its shadow. Results can be seen in Fig. 22, where simulation 1 refers to a simulation with smooth beam screen, and simulation 2 to a simulation with a localized aperture restriction. Since the impact angle of particles varies roughly linearly along the length of the quadrupole magnet, the shifting of the distribution implies an increase by 100% of the average impact angle of protons on the beam screen.

3. Particle-shower simulation

In the static orbit-bump quench test the magnet quenched from a near constant particle loss rate of about 3×10^8 protons/s. Figure 23 shows the transverse profile of power density at maximum along the longitudinal axis for smooth surface. Since the loss distribution is similar to that of the intermediate-duration orbit-bump quench test, the power density profile is also similar. The maximum power density occurs in the internal coil of the magnet and is about 41 mW/cm^3, averaged over the cable cross section. The comparison of predicted and measured BLM signals, as well as the corresponding power deposition in the coil, is shown in Fig. 22. The second simulation, assuming a localized aperture restriction, yielded an 80% higher maximum power density mainly due to the increase in impact angle of the lost protons.

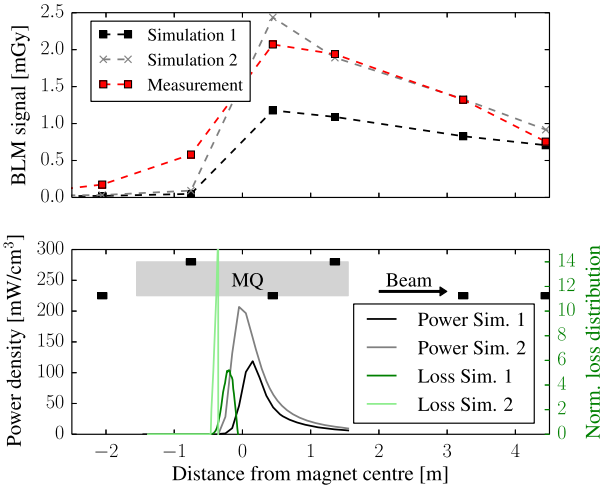

FIG. 22. Results of particle-tracking and particle-shower simulations. Simulation 1 considers a smooth beam screen, whereas simulation 2 considers a 20-cm-long, 30-μm-high aperture restriction close to the magnet center. Up: Detail of the comparison between the BLM signal and the simulated signal from FLUKA for the static orbit-bump quench test. Down: FLUKA simulated peak energy density (black) deposited in the coils and MAD-X normalized distribution of protons lost on the beam screen (green). The gray box indicates the magnet, black boxes indicate the locations of BLMs.

4. Electrothermal simulation

Two alternative models were used for steady-state cooling, differing in the assumption on the effectiveness of the interlayer cooling channels in the MQ. Results are displayed in Table VIII. Note that the first attempt has not been simulated by MAD-X and FLUKA. The displayed values are rescaled by use of the BLM signals in Fig. 19. We estimate the uncertainty introduced by this scaling to be 10%. The more conservative assumptions give the better agreement with the FLUKA analysis and are, therefore, used as the baseline.

As the test featured the longest duration of continuous losses of all studied events, another explanation of the low quench level has been suggested: that the quench level is determined not by the heat transport through the cable insulation, but by the heat transport towards the heat exchanger, thus, requiring the modeling of an entire magnet cross section, rather than just a turn in the coil. Further studies in this direction will be carried out, in continuation of previous work [63,64].

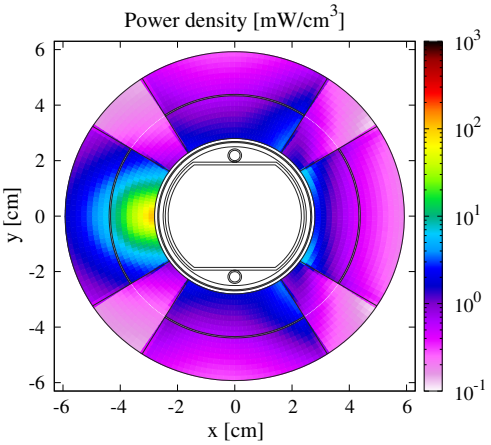

FIG. 23. Simulated transverse power density distribution during the static orbit-bump quench test in MQ.12L6 coils at the location where the maximum energy deposition occurs. Results correspond to 3×10^8 protons impacting on the magnet beam screen.

TABLE VIII. Quench-level comparison; FLUKA and the electrothermal MQPD estimate for the static orbit-bump quench test. Simulations 1 and 2 correspond to MAD-X models without and with an aperture restriction, respectively; compare with Fig. 22. The upper and lower values for the electrothermal estimate correspond to a cooling model with and without heat flow through the intralayer spacers, respectively.

Attempt	Simulation	Particle shower [mW/cm^3]	Electrothermal [mW/cm^3]
1st	1	>36	80–100
1st	2	>61	80–100
2nd	1	43	70–88
2nd	2	72	70–88

5. Discussion

The slow blowup of the beam, generated with the ADT transverse damper, was effective in generating near steady-state losses over 20 s, strong enough to eventually quench an MQ magnet. The test represents, therefore, a good benchmark for the steady-state electrothermal models. The sizable discrepancy between measured and simulated BLM signals led to a comprehensive parametric study in the particle-tracking simulations. An aperture restriction on the scale of several tens of micrometers could best account for the discrepancy. To confirm or rule out this explanation, a repetition of the test would have to be carried out in a different location.

VII. CONCLUSIONS AND OUTLOOK

A. Summary of quench tests

The large-kick event and the short-duration collimation quench test are interesting benchmarks for the particle-tracking and particle-shower simulations, because the electrothermal MQED estimate is not expected to have a sizable error as a consequence of the negligible contribution of heat transfer processes. The large-kick event indeed confirmed the MQED estimate. The collimation quench test led to a 50% overestimation of the MQED estimate by the FLUKA result. This is likely due an inaccuracy in the FLUKA geometrical model. Without meaningful BLM signals (saturated channels), however, there is no clear indication where to search for such a discrepancy. The 50% error must, thus, be regarded as a measure of the error that may affect other FLUKA analyses in the absence of validation data.

In the intermediate-duration regime we note that a precise timing and an adequate time resolution of signals is of paramount importance. Future tests in this regime should include synchronous measurement of BLM, QPS, and FBCT signals. For a better understanding of intermediate-duration losses due to dust particles, a test should create millisecond losses with a smooth time distribution in an MB or MQ magnet (at 1.9 K). The orbit-bump quench test featured losses that peaked of several tens of microseconds every three to four turns of the excited bunch. It is suspected that this substructure of short loss spikes has led to the surprisingly high quench level, 4 times above the expected one.

The testing of quench levels in the steady-state regime is of importance, for example, for the strategies for future collimation upgrades. In this sense the empirical result of the collimation quench test (no quench for 5.8 MJ on the primary collimator within 15 s) gives actionable information and the test will be repeated at higher beam energies for protons and ions. Based on the dynamic and static orbit-bump quench tests, we conclude that the semiempirical steady-state cooling model seems to suggest that interlayer spacers are not having a large effect on the steady-state quench level. An overview of the analysis results is given in Table IX.

B. Impact on quench level estimates

For single-turn losses, i.e., losses of nanosecond duration, we have learned to trust the electrothermal model, which is based on the strand enthalpy margin. Note, however, that for the operation of the LHC, the shortest duration that is resolved by the BLM system is 40 μs. Based on the intermediate-duration orbit-bump quench test we should revise our quench-level estimate upward by a factor 4 in the millisecond time range. The analysis of the quench test has given room for speculation that the high observed quench level may be due to the temporal substructure of the beam loss. If losses of microsecond duration are cooled much more efficiently than slower losses, this would be an indication that also the quench-level estimates in the microsecond range need to be revised upwards. Moreover, it is not clear how this uncertainty scales up to higher energies. We use the same factor 4 at 7 TeV as for 4 TeV.

As for steady-state losses, the testing of the semiempirical model used in the electrothermal estimates is not quite conclusive. Whereas the dynamic orbit-bump test seems to indicate a larger quench level, the static orbit-bump test points to lower levels. This could be due to a low efficiency of the intralayer spacer's cooling channels, or due to different bottleneck in the heat transfer to the heat exchanger tube. Additional numerical and experimental studies are required. Moreover, it must be noted that the semiempirical model is based on measurements on cable stacks with the insulation scheme of LHC main magnets. Quadrupoles and separation dipoles in the dispersion suppressor, matching section, and inner-triplet region are equipped with different insulation schemes. Clearly, a direct use of the present model for those magnet types is doubtful.

Figure 24 provides a summary of the lessons learned for quench levels. The shaded areas represent the uncertainty ranges of our numerical models at 3.5 and 7 TeV for

TABLE IX. Overview of the presented analyses. BLM validation indicates the level of agreement between particle-tracking and particle-shower simulations with BLM data. Quench-level consistency indicates the agreement between quench-level data obtained from particle-shower simulation results with the electrothermal estimates. "Good" indicates agreement within 20%–30%, "average" around 50%, and "poor" larger than 100%.

Regime	Method	Type	Temperature [K]	I/I_{nom} [%]	BLM validation	Quench level consistency	Sources of uncertainty
Short	Kick	MB	1.9	6	Good	Good	Tracking uncertainty
Short	Collimation	MQM	4.5	46/58	···	Average	Saturated BLM signals. No FLUKA validation.
Intermediate	Wire scanner	MBRB	4.5	50	Good	Average	Timing uncertainty. Quench in magnet end.
Intermediate	Wire scanner	MQY	4.5	50	Good	Consistent	No quench.
Intermediate	Orbit bump	MQ	1.9	54	Good	Poor	Timing uncertainty. Inaccurate heat-transfer model. No quench. Peak loss in magnet end.
Steady-state	Collimation	MB	1.9	57	Poor	Consistent	Moderate FLUKA agreement with BLM signals. Intralayer spacer cooling efficiency. Sensitivity to surface roughness.
Steady-state	Static orbit bump	MQ	1.9	54	Average	Average	Intralayer spacer cooling efficiency.
Steady-state	Dynamic orbit bump	MQ	1.9	0.47	Good	Good	Intralayer spacer cooling efficiency.

rectangular loss pulses of durations in the intermediate-duration and steady-state regimes. The solid lines indicate the new baseline for the setting of BLM thresholds. For intermediate-duration losses, the more progressive branch was selected, which is in line with the results of the intermediate-duration orbit-bump quench test. For the steady-state regime, the more conservative branch was chosen, which is in line with the static orbit-bump quench test. For magnet types that have not been tested with steady-state quench tests, such as the matching-section quadrupoles, the separation dipoles, and the triplet quadrupoles, an even more conservative model was retained, representing the cable insulation as a solid layer of Kapton, thus, neglecting any aid to heat transport through the insulation, by the superfluid helium.

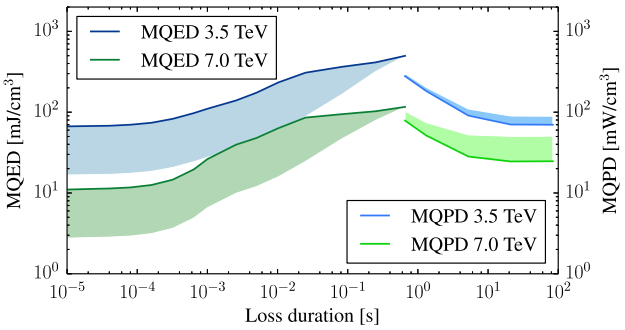

FIG. 24. Electrothermal quench level estimates for the inner layer of the LHC main bending magnet. Shading in the MQED estimates indicates uncertainties following from the analysis of the intermediate-duration orbit-bump quench test. Shading in the MQPD estimates indicates uncertainties due to the unknown cooling efficiency of intralayer spacers in the main magnets of the LHC.

C. Future tests

Quench tests and beam-loss events during run 1 have substantially improved our understanding of various beam-loss scenarios, and of the quench levels of main magnets in the LHC. We have shown that, based on good knowledge of the initial conditions and on validation data, the numerical models reproduce beam-loss events to a remarkable degree. Based on this new-found confidence, quench tests can be considered one of the most accurate means to test and validate electrothermal estimates of quench levels under realistic conditions.

For single-turn losses, which are relevant, for example, in the case of asynchronous beam dumps, another collimator quench-test analogous to the test on the Q6 magnet described in Sec. IV B is under preparation. To improve the model validation, beam-loss monitors with higher sensitivity and dynamic range will be used.

In the intermediate-duration regime, during run 2 of the LHC a significant number of beam losses due to collisions of the proton beam with dust particles may provoke beam-induced quenches. Based on the knowledge of beam parameters and particle-shower models, the corresponding

BLM data will allow one to obtain additional information of quench levels in the relevant time range. To prepare for the need of a controlled quench test with diagnostic equipment (oscilloscope, etc.), we are studying the possibility of causing losses in the millisecond regime through a combination of a local orbit bump in a main quadrupole and a fast current decay in a warm dipole leading to an orbit distortion [39].

Finally, for steady-state losses we advocate the repetition of the static orbit-bump quench test in a different location in the arc to better understand the discrepancies observed in analysis of the first test of this type. A repetition could confirm or rule out the presence of a small geometrical obstruction that may have influenced the outcomes of the first test. Moreover, we suggest to repeat the test in standalone quadrupoles with different insulation schemes, such as MQM, MQY, MQXA, and MQXB types. In the absence of additional subscale experiments, these tests could provide information on the steady-state cooling efficiency in those magnet types.

In 2013 there was not the opportunity to execute the steady-state collimation quench tests with ions. A dedicated test in run 2 will allow one to directly determine the quench limit for this loss scenario. The same approach should be followed for a proton collimation quench test at increased beam energy; the result of this test provides direct input for the optimized setting of BLM thresholds, the minimum allowed beam lifetime, and on the collimator upgrade for high luminosity LHC.

D. Conclusion

The preparation and organization of quench tests and the analysis of beam-loss events have been highly collaborative and multidisciplinary efforts, stretching over the past several years. We have found that, with good knowledge of initial conditions and sufficient data for validation, particle-tracking and particle-shower simulations provide, in the best cases, results in 20% agreement with BLM signals in the region of peak losses. This level of accuracy allows one to make quantitative statements on the range of validity of electrothermal quench-level estimates. The gained knowledge on beam-loss scenarios and quench levels is currently being applied in the setting of BLM thresholds in the LHC for run 2.

[1] M. Sapinski *et al.*, Beam induced quenches of LHC magnets, in *Proceedings of the 4th International Particle Accelerator Conference, IPAC-2013, Shanghai, China, 2013* (JACoW, Shanghai, China, 2013), THPEA045, pp. 3243–3245.

[2] K. Wittenburg, Beam losses and machine protection, DESY internal note, Report No. HERA-05-01, (2005).

[3] A. Valishev *et al.*, Tevatron accelerator physics and operation highlights, in *Proceedings of the 24th Particle Accelerator Conference, PAC-2011, New York, 2011* (IEEE, New York, 2011), MOONCN2, pp. 37–40.

[4] M. Bai *et al.*, Beam losses and beam-induced quenches at BNL, in *Proceedings of the 2014 Workshop on Beam-Induced Quenches, Geneva, Switzerland, 2014*.

[5] J. B. Jeanneret *et al.*, Quench levels and transient beam losses in LHC magnets, LHC Project Report No. 044, 1996.

[6] H. Edwards, C. Rode, and J. McCarthy, Measurements of magnet quench levels by proton beam spray, IEEE Trans. Magn. **13**, 666 (1977).

[7] M. Sapinski *et al.*, Beam-induced quench tests of LHC magnets, in *Proceedings of IPAC 2014, Dresden, Germany, MOOCB01*, pp. 52–54.

[8] G. Frei *et al.*, Void fraction, interstrand contact area and free strand surface area in an LHC Rutherford cable, *The ASC Conference, Chicago, USA, 2008.*

[9] A. Verweij, QP3: Users manual, CERN/TE, EDMS 1150045, 2008.

[10] M. Sapinski *et al.*, Simulation of beam loss in LHC MB magnet and quench threshold test, Report No. LHC-Project-Note-422, 2009.

[11] W. Herr and F. Schmidt, A MAD-X primer, CERN AB Note, Report No. CERN-AB-2004-027-ABP, 2004.

[12] F. Schmidt, SixTrack, users reference manual, CERN Report No. SL/94-56 (AP), 1994, updated 2008.

[13] A. Fasso *et al.*, FLUKA: A multi-particle transport code, Reports No. CERN-2005-10, No. INFN/TC_05/11, and No. SLAC-R-773, 2005.

[14] G. Battistoni *et al.*, The FLUKA code: Description and benchmarking, in *Proceedings of the Hadronic Shower Simulation Workshop 2006 at Fermilab, Batavia, IL, USA* [*AIP Conf. Proc.* 896, 31 (2007)].

[15] S. Agostinelli *et al.*, Geant4: A simulation toolkit, Nucl. Instrum. Methods Phys. Res., Sect. A **506**, 250 (2003).

[16] A. Lechner *et al.*, Validation of energy deposition simulations for TeV proton losses in the CERN Large Hadron Collider (to be published).

[17] L. Bottura, THEA thermal, hydraulic and electric analysis of superconducting cable, CryoSoft, 1.3 edition, 2003.

[18] L. Bottura, ZeroDee, http://www.htess.com/cryosoft.htm, 2013.

[19] P. Bauer, Stability of superconducting strands for accelerator magnets, Ph.D. thesis, Technical University Vienna, 1996.

[20] CERN TE/MSC, ROXIE, http://cern.ch/roxie/, 2013.

[21] P. Bauer, Stability of superconducting strands for accelerator magnets, Ph.D. thesis, Technical University Vienna, Austria, 1996.

[22] P. P. Granieri, M. Calvi, P. Xydi, B. Baudouy, D. Bocian, L. Bottura, M. Breschi, and A. Siemko, Stability analysis of the LHC cables for transient heat depositions, IEEE Trans. Appl. Supercond. **18**, 1257 (2008).

[23] G. Willering, Stability of superconducting Rutherford cables, Ph.D. thesis, University of Twente, Netherlands, 2009.

[24] J. Depond *et al.*, Superconducting cable topology, LHC– AT/MMS Internal Note No. 97-09, 1997.

[25] D. Richter, J. Fleiter, B. Baudouy, and A. Devred, Evaluation of the transfer of heat from the coil of the LHC dipole magnet to helium II, IEEE Trans. Appl. Supercond. **17**, 1263 (2007).

[26] P. P. Granieri, P. Fessia, D. Richter, and D. Tommasini, Heat transfer in an enhanced cable insulation scheme for the superconducting magnets of the LHC luminosity upgrade, IEEE Trans. Appl. Supercond. **20**, 168 (2010).

[27] P. P. Granieri and R. van Weelderen, Deduction of steady-state cable quench limits for various electrical insulation schemes with application to LHC and HL-LHC magnets, IEEE Trans. Appl. Supercond. **24**, 4802806 (2014).

[28] P. P. Granieri, Steady-state heat transfer in the LHC superconducting coils: Status of experiments and modelling, *The 2014 Workshop on Beam-Induced Quenches*, http://indico.cern.ch/event/BIQ2014, 2014.

[29] A. Priebe, Quench tests of LHC magnets: Studies on beam-loss development and determination of quench levels, Ph.D. thesis, EPFL Lausanne, Switzerland, 2014.

[30] A. Lechner *et al.*, Energy deposition studies for fast losses during LHC injection failures, in *Proceedings of the 4th International Particle Accelerator Conference, IPAC-2013, Shanghai, China, 2013* (Ref. [1]), TUPFI027, pp. 1397–1399.

[31] B. Auchmann *et al.*, Quench and damage levels for Q4 and Q5 magnets near point 6, CERN TE-MPE Technical Note No. 01-2014, 2014.

[32] C. Bracco *et al.*, Test and simulation results for quenches induced by fast losses on a LHC quadrupole, in *Proceedings of IPAC2014, Dresden, Germany* (2014), WEPRI092, pp. 2706–2708.

[33] National Institute of Standards and Technology (NIST), Cryogenics material properties database, http://www.cryogenics.nist.gov/MPropsMAY/material%20properties.htm (2014).

[34] E. D. Marquardt *et al.*, *Cryogenic Material Properties Database, in Cryocoolers 11(11)*, edited by R. J. Ross Jr. (Kluwer Academic Publishers, New York, 2001), pp. 689–699.

[35] C. Bracco *et al.*, Experiments on the margin of beam induced quenches for LHC superconducting quadrupole magnet, in *Proceedings of the 3rd International Particle Accelerator Conference, New Orleans, LA, 2012* (IEEE, Piscataway, NJ, 2012), MOPPC004, pp. 124–126.

[36] T. Baer *et al.*, UFOs in the LHC, in *Proceedings of the 2nd International Particle Accelerator Conference, San Sebastián, Spain* (EPS-AG, Spain, 2011), TUPC137, pp. 1347–1349.

[37] T. Baer *et al.*, UFOs in the LHC: Observations, studies, and extrapolations, in *Proceedings of the 3rd International Particle Accelerator Conference, New Orleans, LA, 2012* (Ref. [36]), THPPP086, pp. 3936–3938.

[38] E. Nebot *et al.*, Analysis of fast losses in the LHC with the BLM system, in *Proceedings of the 2nd International Particle Accelerator Conference, San Sebastián, Spain* (Ref. [37]), TUPC136, pp. 1344–1346.

[39] T. Baer, Very fast losses of the circulating LHC beam, their mitigation and machine protection, Ph.D. thesis, Universität Hamburg, 2013.

[40] A. Lechner, BLM signals induced by beam-dust particle interactions in the LHC arcs, *The LHC Machine Protection Panel, 2013*.

[41] A. Gomez Alonso, Redundancy of the LHC machine protection systems in case of magnet failures, Ph.D. thesis, Universitat Politècnica de Catalunya Barcelona, Spain, 2009.

[42] M. Sapinski *et al.*, LHC magnet quench test with beam loss generated by wire scan, in *Proceedings of the 2nd International Particle Accelerator Conference, San Sebastián, Spain* (Ref. [37]), WEPC173, pp. 2391–2394.

[43] M. Sapinski *et al.*, Carbon fiber damage in particle beam, *46th ICFA Advanced Beam Dynamics Workshop on High-Intensity and High-Brightness Hadron Beams, Morschach, Switzerland, MOPD61* (JACOW, 2010), pp. 231–234.

[44] W. Höfle *et al.*, Controlled transverse blow-up of high energy proton beams for aperture measurements and loss maps, in *Proceedings of the 3rd International Particle Accelerator Conference, New Orleans, LA, 2012* (Ref. [36]), THPPR039, pp. 4059–4061.

[45] M. Sapinski *et al.*, Generation of millisecond controlled losses with transverse damper on LHC, in *Proceedings of the 4th International Particle Accelerator Conference, IPAC-2013, Shanghai, China, 2013* (Ref. [1]), WEPME044, pp. 3025–3028.

[46] V. Chetvertkova *et al.*, MAD-X tracking simulations to determine the beam-loss distributions for the LHC quench tests with ADT excitation, in *Proceedings of IPAC2014, Dresden, Germany* (2014), THPRI094, pp. 3991–3994.

[47] N. Shetty *et al.*, Energy deposition and quench level calculations for millisecond and steady-state quench tests of LHC arc quadrupoles at 4 TeV, in *Proceedings of IPAC2014, Dresden, Germany* (2014), MOPRO019, pp. 105–108.

[48] C. Schmidt, Stability of superconductors in helium I and helium II, in *Stability of Superconductors* (International Institute of Refrigeration Commission A 1/2, Saclay, 1981), pp. 17–32.

[49] D. Wollmann *et al.*, Collimator losses in the DS of IR7 and quench test at 3.5 TeV, CERN Internal Note, CERN-ATS-Note-2011-042 MD, 2011.

[50] G. Bellodi *et al.*, Pb ions collimator losses in IR7 DS and quench test at 3.5 Z TeV, CERN Internal Note, Report No. CERN-ATS-Note-2012-081 MD, 2012.

[51] O. Brüning *et al.*, LHC design report volume 1: The LHC main ring, CERN, 2004.

[52] R. W. Assmann, Collimators and beam absorbers for cleaning and machine protections, in *Proceedings of the 2nd LHC Project Workshop - Chamonix XIV*, edited by J. Poole (CERN, Geneva, 2005), pp. 261–267.

[53] R. W. Assmann *et al.*, The final collimation system for the LHC, in *Proceedings of the 10th European Particle Accelerator Conference, Edinburgh, Scotland, 2006* (EPS-AG, Edinburgh, Scotland, 2006), TUODFI01, pp. 986–988.

[54] D. Wollmann *et al.*, First cleaning with LHC collimators, in *Proceedings of the International Particle Accelerator Conference, Kyoto, Japan* (ICR, Kyoto, 2010), TUOAMH01, pp. 1238–1239.

[55] D. Wollmann *et al.*, Collimator losses in the DS of IR7 and quench test at 3.5 TeV, CERN Internal Note, Report No. CERN-ATS-Note-2011-042 MD, 2011.

[56] B. Salvachua *et al.*, Collimation quench test with 4 TeV proton beams, CERN Internal Note, Report No. CERN-ACC-NOTE-2014-0036, 2014.

[57] T. Trenkler and J. B. Jeanneret, K2, a software package evaluating collimation systems in circular colliders (manual), CERN Internal Note, Report No. SL/94-105 (AP), 1994.

[58] G. Robert-Demolaize *et al.*, A new version of SixTrack with collimation and aperture interface, in *Proceedings of the 21st Particle Accelerator Conference, Knoxville, TN, 2005* (IEEE, Piscataway, NJ, 2005), TPAP007, pp. 4084–4086.

[59] R. Bruce *et al.*, Simulation and measurements of beam-loss patterns at the CERN Large Hadron Collider, Phys. Rev. ST Accel. Beams **17**, 081004 (2014).

[60] E. Skordis *et al.*, Impact of beam losses in the LHC collimation regions, in *Proceedings of IPAC 2015, Richmond, USA* (2015), TUPTY046.

[61] A. Priebe *et al.*, Beam-induced quench test of a LHC main quadrupole, in *Proceedings of the 2nd International Particle Accelerator Conference, San Sebastián, Spain* (Ref. [37]), WEPC172, pp. 2388–2390.

[62] A. Priebe, B. Dehning, M. Sapinski, M. Q. Tran, and A. Verweij, Investigations of quench limits of the LHC superconducting magnets, IEEE Trans. Appl. Supercond. **23**, 4701205 (2013).

[63] D. Bocian, B. Dehning, and A. Siemko, Modeling of quench limit for steady state heat deposits in LHC magnets, IEEE Trans. Appl. Supercond. **18**, 112 (2008).

[64] R. Bruce, D. Bocian, S. Gilardoni, and J. M. Jowett, Beam losses from ultraperipheral nuclear collisions between 208Pb82+ ions in the large hadron collider and their alleviation, Phys. Rev. ST Accel. Beams **12**, 071002 (2009).